IEEE Access
Multidisciplinary : Rapid Review : Open Access Journal

Received 19 May 2023, accepted 1 June 2023, date of publication 5 June 2023, date of current version 19 June 2023.

Digital Object Identifier 10.1109/ACCESS.2023.3282994

RESEARCH ARTICLE

A Synthesis Method for *N*-Section Unequal Ultra-Wideband Wilkinson Power Divider With Controllable Equal-Ripple Performance

ZIZHUO SUN[1], (Graduate Student Member, IEEE), XIAOLONG WANG[1], (Member, IEEE), LEI ZHU[2], (Fellow, IEEE), AND GEYU LU[1]

[1]State Key Laboratory of Integrated Optoelectronics, College of Electronic Science and Engineering, Jilin University, Changchun 130012, China
[2]Department of Electrical and Computer Engineering, University of Macau, Macau, China

Corresponding author: Xiaolong Wang (brucewang@jlu.edu.cn)

This work was supported in part by the National Natural Science Foundation of China under Grant 62271229, in part by the Project of Jilin Province Development and Reform Commission under Grant 2022C047-6, in part by the Project of Science and Technology Development Program of Changchun City under Grant 21ZY23, and in part by the Interdisciplinary Integration and Innovation Project of Jilin University (JLU) under Grant JLUXKJC2020204.

ABSTRACT In this paper, a novel synthesis method is presented to design of a class of multi-section ultra-wideband (UWB) Wilkinson power dividers (WPDs) with an arbitrary power ratio. The proposed UWB-WPD topology consists of N cascaded asymmetric coupled line sections (ACLSs) and N isolation resistors. Through even- and odd-mode analysis, the proposed synthesis method is demonstrated with a few unique novelties as summarized: (1) It is for the first time proved that the first kind Chebyshev equal-ripple performance can be exactly realized by the cascaded transmission-line transformer without Hansen's approximation; (2) It is also for the first time revealed that all the S-parameters ($S_{11}, S_{21}, S_{31}, S_{22}, S_{33}$ and S_{32}) of proposed WPD can achieve controllable in-band equal-ripple performance. To verify the effectiveness of proposed synthesis method, several design examples are presented and designed for demonstration of varied equal-ripple responses. Finally, two WPD circuits with $N = 3$ are fabricated, and the measured results well validate the predicted ones from proposed method.

INDEX TERMS Asymmetric coupled line section (ACLS), first-kind Chebyshev frequency response, ultra-wideband (UWB), Wilkinson power divider (WPD).

I. INTRODUCTION

Wilkinson power divider (WPD) [1] has been widely used as a basic microwave passive component in modern wireless communication systems. Excellent isolation between two output ports and perfect impedance matching at all the ports can be simultaneously achieved at the center frequency. Suffering from the intrinsic limited bandwidths, multi-section WPD [2] has been reported to meet the increased demand in wideband wireless communications.

So far, a variety of WPDs with different configurations have been developed to improve the operating bandwidth, enhance the isolation and miniaturize the circuit size [3], [4], [5], [6], [7], where the parallel-coupled line sections and open-circuited stubs are replaced by two quarter-wave transmission lines to realize wideband power ratio performance, while a single isolation resistor is maintained for wideband isolation. Considering circuit miniaturization, several ultra-wideband (UWB) power dividers with MMIC process [8], GaAs pHEMT process [9], SiGe BiCOMS process [10] have been reported. Later on, an alternative class of wide-band WPDs [11], [12], [13] has been implemented by the lumped elements, resulting to not only remarkably attain compact circuit size, but also effectively enhance harmonic suppression. However, all the aforementioned WPD topologies are difficult to be applied in high frequency bands, due to the following two reasons: (1) As frequency increases, all the lumped elements gradually become frequency-depended;

The associate editor coordinating the review of this manuscript and approving it for publication was Mohamed Kheir.

(2) All the parasitic effects involved in these lumped elements are too complicated to be accurately analyzed and effectively controlled. As a result, these lumped-element WPDs cannot satisfactorily realize wide passband performance as theoretically predicted, especially in high frequencies. Although microstrip-to-slotline transitions could be used to solve the above problem in wideband WPDs [14], [15], multi-layer structure is not preferred for low cost and easy fabrication. By using different wideband techniques such as ring resonators [16], multilayer slotline [17], transversal signal-interference sections [18], shunted stubs and coupled line sections [19], [20], [21], [22], bandpass responses of wideband WPDs can be attained. Furthermore, dual-wideband [23], [24] or even tunable WPD with filtering function [25], [26] can be realized.

By summarizing the relationship between voltage standing wave ratio (VSWR) and first-kind Chebyshev polynomial, Cohn reported a broadband stepped transmission-line transformer (TLT) [27], Hansen's approximation was also introduced to optimize quasi-equal-ripple performance. Then, this method has been widely used in multi-section WPD design [28], [29], [30]. In this context, various optimization approaches have been reported nowadays to improve the wideband performance of WPDs [28], [29], [30], [31], [32], [33], [34]. But, to the best of the authors' knowledge, the following key problems have not been solved in multi-section WPD: (1) No synthesis theory is available to design exactly the first kind Chebyshev equal-ripple response of S_{11}; (2) Reflection coefficients (S_{22}, S_{33}) and transmission coefficient (S_{32}) can hardly achieve equal-ripple responses, and their ripple levels are all uncontrollable in the desired ranges under the condition of arbitrary power ratio. To sum up, no design method is developed so far to realize equal-ripple performance and controllable ripple levels in WPD design.

In this paper, a novel synthesis method is firstly presented in the proposed wideband WPD topology, where it consists of N cascaded asymmetric coupled line sections (ACLSs) and N isolation resistors. Each isolation resistor is shunted on the right side of its ACLS. The power ratio between two output ports can be selected arbitrarily. Although the similar topologies have been reported in the previous works [28], [29], [30], the proposed wideband WPD can offer the following unique features by virtue of the novel synthesis method: (1) It is for the first time proved that the first-kind Chebyshev equal-ripple performance can be exactly realized by virtue of the cascaded TLT without Hansen's approximation [22], the detailed improvements are listed in Appendix for verification. (2) Compared with the former work in [22], the numbers and frequencies of output-ports reflection zeros ($S_{22} = S_{33} = 0$)/isolation zeros ($S_{32} = S_{23} = 0$) can also exactly match with those of input-port reflection zeros ($S_{11} = 0$) under the condition of unequal power ratio. (3) It is also for the first time revealed that all the S-parameters (S_{11}, S_{21}, S_{31}, S_{22}, S_{33} and S_{32}) of proposed WPD can provide equal-ripple performance and controllable ripple levels. As we know so far, no method has been presented to realize equal-ripple, matched reflection/isolation zeros and controllable ripple levels for all the reflection and transmission coefficients, as can be found from many previous works [3], [4], [5], [6], [7], [8], [9], [10], [11], [12], [13], [14], [15], [16], [17], [18], [19], [20], [21], [22], [23], [24], [25], [28], [29], [30], [31], [32], [33], [34]. After several WPDs with different functionalities are theoretically designed and demonstrated, two prototype WPDs on the microstrip-line structure are in final fabricated and tested for experimental verification of the proposed synthesis method.

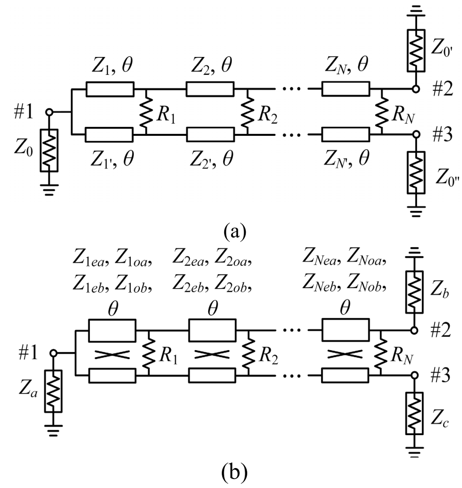

FIGURE 1. The topology of N-section WPD. (a) Conventional WPD with equal power ratio [28], [32] or unequal power ratio [29], [30], [31]. (b) Proposed WPD.

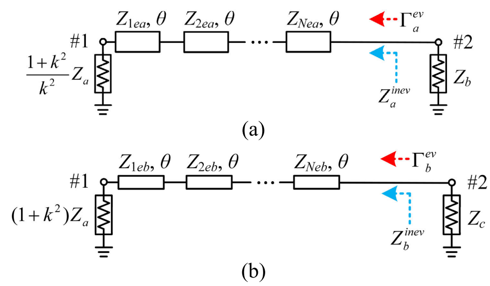

FIGURE 2. The even-mode equivalent bisection circuits for proposed WPD. (a) Upper bisection circuit. (b) Lower bisection circuit.

II. DESIGN METHOD OF PROPOSED WPD

Compared with the former works [28], [29], [30], [31], [32] in Fig. 1 (a), the topology of proposed N-section unequal WPD is shown in Fig. 1 (b), and it consists of N cascaded ACLSs and N isolation resistors. Z_{iea}, Z_{ieb} and Z_{ioa}, Z_{iob} are the even- and odd-mode characteristic impedances of the i-th ACLS (where $i = 1, 2, \ldots, N$), the electrical length of each ACLS is equal to θ. The i-th isolation resistor R_i is shunted on the right side of i-th ACLS. The power ratio between port 2 and port 3 is expressed as k^2. Z_a, Z_b, Z_c are three terminal load impedances, where $Z_c/Z_b = k^2$. When $k^2 = 1$, the proposed topology becomes equal WPD.

A. EVEN-MODE ANALYSIS

Fig 2 (a) and (b) show the even-mode equivalent circuits of proposed WPD. Since all the parameters of the upper bisection circuit in Fig 2 (a) are $1/k^2$ times the corresponding parameters of the lower circuit in Fig 2 (b), only the upper bisection circuit needs to be discussed in even-mode analysis.

The *ABCD* matrix of the i-th ACLS in Fig.2 (a) is deduced as

$$\begin{bmatrix} A_{iea} & B_{iea} \\ C_{iea} & D_{iea} \end{bmatrix} = \begin{bmatrix} \cos\theta & jZ_{iea}\sin\theta \\ j\sin\theta/Z_{iea} & \cos\theta \end{bmatrix} \tag{1}$$

Then, the entire *ABCD* matrix of the upper ACLSs can be derived by multiplying the *ABCD* matrices of cascaded sections, such that.

$$\begin{bmatrix} A_a^{ev} & B_a^{ev} \\ C_a^{ev} & D_a^{ev} \end{bmatrix} = \begin{bmatrix} A_{Nea} & B_{Nea} \\ C_{Nea} & D_{Nea} \end{bmatrix} \begin{bmatrix} A_{(N-1)ea} & B_{(N-1)ea} \\ C_{(N-1)ea} & D_{(N-1)ea} \end{bmatrix} \cdots \begin{bmatrix} A_{1ea} & B_{1ea} \\ C_{1ea} & D_{1ea} \end{bmatrix} \tag{2}$$

After complicated arithmetical operation the equations in (2) can be simplified as

$$A_a^{ev} = \sum_{n=0}^{\frac{N-W}{2}} a_{(2n+W)e}^{re} \cos^{2n+W}\theta \tag{3a}$$

$$B_a^{ev} = \frac{j}{\sin\theta} \sum_{n=0}^{\frac{N+W}{2}} b_{(2n+1-W)e}^{im} \cos^{2n+1-W}\theta \tag{3b}$$

$$C_a^{ev} = \frac{j}{\sin\theta} \sum_{n=0}^{\frac{N+W}{2}} c_{(2n+1-W)e}^{im} \cos^{2n+1-W}\theta \tag{3c}$$

$$D_a^{ev} = \sum_{n=0}^{\frac{N-W}{2}} d_{(2n+W)e}^{re} \cos^{2n+W}\theta \tag{3d}$$

where, $W = \mathrm{sgn}(N \bmod 2)$, $a_{(2n+W)e}^{re}$ and $d_{(2n+W)e}^{re}$ are polynomial functions with the degree $(2n+W)$, where $n = 0, 1, 2, \ldots, (N-W)/2$; $b_{(2n+1-W)e}^{im}$ and $c_{(2n+1-W)e}^{im}$ are polynomial functions with the degree $(2n+1-W)$, where $n = 0, 1, 2, \ldots, (N+W)/2$.

Because $a_{(2n+W)e}^{re}$, $b_{(2n+W-1)e}^{im}$, $c_{(2n+W-1)e}^{im}$ and $d_{(2n+W)e}^{re}$ are only determined by the characteristic impedances Z_{iea} ($i = 1, 2, \ldots, N$), the input impedance of port 2 Z_a^{inev} can be derived as

$$Z_a^{inev} = \frac{\left(1+k^2\right) Z_a \cdot A_a^{ev} + k^2 B_a^{ev}}{\left(1+k^2\right) Z_a \cdot C_a^{ev} + k^2 D_a^{ev}} \tag{4}$$

In even-mode analysis, reflection coefficient Γ_a^{ev} at port 2 is

$$\Gamma_a^{ev} = \left(Z_a^{inev} - Z_b\right) \Big/ \left(Z_a^{inev} + Z_b\right) \tag{5}$$

Then, S_{11}, S_{21} and S_{31} can be summarized as

$$S_{11} = \left(\Gamma_a^{ev} + \Gamma_b^{ev}\right)/2 = \Gamma_a^{ev} = S_{11ea} \tag{6a}$$

$$S_{21} = kS_{21ea} \Big/ \sqrt{1+k^2} \tag{6b}$$

$$S_{31} = S_{21ea} \Big/ \sqrt{1+k^2} \tag{6c}$$

where

$$S_{21ea} = \frac{2k\sqrt{\left(1+k^2\right) Z_a Z_b}}{\left(1+k^2\right) Z_a A_a^{ev} + k^2 B_a^{ev} + \left(1+k^2\right) Z_a Z_b C_a^{ev} + k^2 Z_b D_a^{ev}} \tag{6d}$$

$F_{circuit}$ is defined as the characteristic function of proposed circuit. From $|S_{21}|^2 + |S_{31}|^2 = 1 - |S_{11}|^2$ (lossless), we have

$$|F_{circuit}|^2 = |S_{11}|^2 \Big/ \left(|S_{21}|^2 + |S_{31}|^2\right) = \left|S_{11ea}/S_{21ea}\right|^2 \tag{7}$$

Substituting (6a) and (6d) into (7), we have

$$\begin{aligned} F_{circuit} &= \frac{\left(1+k^2\right) Z_a A_a^{ev} + k^2 B_a^{ev} - \left(1+k^2\right) Z_a Z_b C_a^{ev} - k^2 Z_b D_a^{ev}}{2k\sqrt{\left(1+k^2\right) Z_a Z_b}} \\ &= \sqrt{10^{(-RL^{S11}/10)}} \Big/ \sqrt{1 - 10^{(-RL^{S11}/10)}} \end{aligned} \tag{8}$$

where, RL^{S11} is the return loss of S_{11} in decibel.

On the other hand, $F_{formula}$ is defined as the theoretical characteristic function. Based on the synthesis method in [35], the theoretical first-kind Chebyshev transfer function for a lossless two-port circuit is expressed as

$$\left|S_{21formula}(\theta)\right|^2 = \frac{1}{1 + \left|F_{formula}\right|^2} = \frac{1}{1 + \varepsilon^2 \left|\cos(N\varphi)\right|^2} \tag{9}$$

where $\varepsilon = \sqrt{10^{0.1L_A} - 1}$, L_A is the in-band ripple level factor.

In order to realize equal-ripple frequency responses of S_{11}, S_{21} and S_{31} in the proposed WPD, $\left|F_{formula}\right|^2 = |F_{circuit}|^2$ must be maintained. Under the condition of $\theta = 0$, we have

$$\begin{cases} F_{formula}(\theta = 0) = \varepsilon \cdot T_N\left(1 \Big/ \cos\theta_c^{S11}\right) \\ F_{circuit}(\theta = 0) = \dfrac{\left(1+k^2\right) Z_a - k^2 Z_b}{2k\sqrt{\left(1+k^2\right) Z_a Z_b}} \end{cases} \tag{10}$$

where $T_N(x)$ is the Chebyshev polynomial of the first kind, θ_c^{S11} is the electrical length at lower cutoff frequency of S_{11}

ε can be derived as

$$\varepsilon = \frac{1}{T_N\left(1/\cos\theta_c^{S11}\right)} \cdot \frac{\left(1+k^2\right) Z_a - k^2 Z_b}{2k\sqrt{\left(1+k^2\right) Z_a Z_b}} \tag{11}$$

Finally, the general simultaneous equations of even-mode analysis are derived as

$$\begin{cases} \mathrm{Re}\left(F_{circuit}\right) = F_{formula} \\ \mathrm{Im}\left(F_{circuit}\right) = 0 \end{cases} \Rightarrow \begin{cases} F_{circuit} = \varepsilon \cdot T_N\left(\cos\theta \Big/ \cos\theta_c^{S11}\right) \\ k^2 B_a^{ev} - \left(1+k^2\right) Z_a Z_b C_a^{ev} = 0 \end{cases} \tag{12}$$

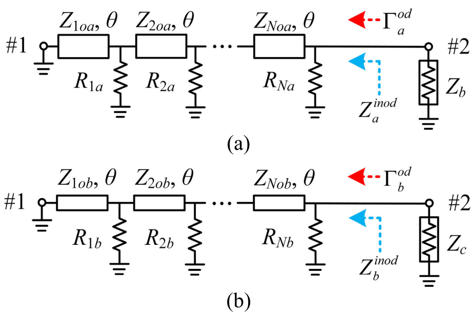

FIGURE 3. The odd-mode equivalent bisection circuits for proposed WPD. (a) Upper bisection circuit. (b) Lower bisection circuit.

It is worth to mentioning that theoretical $F_{formula}$ is newly proved to directly calculate transfer function S_{21} in the even-mode analysis. Then, S_{11}, S_{21} and S_{31} of proposed WPD must provide first-kind Chebyshev equal-ripple responses. Compared with VSWR design method and its Hansen's approximation in [27], the proposed synthesis method of even-mode analysis provides better equal-ripple performance, the detailed differences and improvements are listed and compared in Appendix for verification.

B. ODD-MODE ANALYSIS

Fig 3 (a) and (b) shows the odd-mode equivalent bisection circuits of proposed WPD. Due to the limited pages, only the upper bisection circuit is discussed in this paper.

The *ABCD* matrix of the *i*-th isolation resistor is

$$\begin{bmatrix} A_{Ria} & B_{Ria} \\ C_{Ria} & D_{Ria} \end{bmatrix} = \begin{bmatrix} 1 & 0 \\ 1/R_{ia} & 1 \end{bmatrix} \tag{13}$$

Then, the *ABCD* matrices of the upper bisection circuit can be expressed as

$$\begin{bmatrix} A_a^{od} & B_a^{od} \\ C_a^{od} & D_a^{od} \end{bmatrix} = \begin{bmatrix} 1 & 0 \\ 1/R_{Na} & 1 \end{bmatrix} \begin{bmatrix} A_{Noa} & B_{Noa} \\ C_{Noa} & D_{Noa} \end{bmatrix} \cdots \begin{bmatrix} A_{1oa} & B_{1oa} \\ C_{1oa} & D_{1oa} \end{bmatrix} \tag{14}$$

After complicated arithmetical operation the equations in (14) can be simplified as

$$A_a^{od} = \sum_{n=0}^{\frac{N-W}{2}} a_{(2n+W)o}^{re} \cos^{2n+W}\theta + \frac{j}{\sin\theta} \sum_{n=0}^{\frac{N+W}{2}} a_{(2n+1-W)o}^{im} \cos^{2n+1-W}\theta \tag{15a}$$

$$B_a^{od} = \sum_{n=0}^{\frac{N-W}{2}} b_{(2n+W)o}^{re} \cos^{2n+W}\theta + \frac{j}{\sin\theta} \sum_{n=0}^{\frac{N+W}{2}} b_{(2n+1-W)o}^{im} \cos^{2n+1-W}\theta \tag{15b}$$

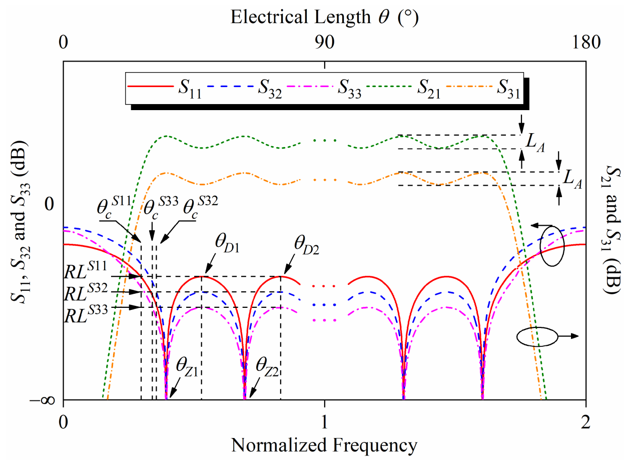

FIGURE 4. Corresponding to the proposed WPD in Fig. 1 (b), a schematic of general *S*-parameters.

$$C_a^{od} = \sum_{n=0}^{\frac{N-W}{2}} c_{(2n+W)o}^{re} \cos^{2n+W}\theta + \frac{j}{\sin\theta} \sum_{n=0}^{\frac{N+W}{2}} c_{(2n+1-W)o}^{im} \cos^{2n+1-W}\theta \tag{15c}$$

$$D_a^{od} = \sum_{n=0}^{\frac{N-W}{2}} d_{(2n+W)o}^{re} \cos^{2n+W}\theta + \frac{j}{\sin\theta} \sum_{n=0}^{\frac{N+W}{2}} d_{(2n+1-W)o}^{im} \cos^{2n+1-W}\theta \tag{15d}$$

where $W = \mathrm{sgn}(N \bmod 2)$, $a_{(2n+W)o}^{re}$, $b_{(2n+W)o}^{re}$, $c_{(2n+W)o}^{re}$ and $d_{(2n+W)o}^{re}$ are polynomial functions with the degree $(2n+W)$, where $n = 0, 1, 2, \ldots, (N-W)/2$; $a_{(2n+1-W)o}^{im}$, $b_{(2n+1-W)o}^{im}$, $c_{(2n+1-W)o}^{im}$ and $d_{(2n+1-W)o}^{im}$ are polynomial functions with the degree $(2n+1-W)$, where $n = 0, 1, 2, \ldots, (N+W)/2$.

Similarly, the input impedance Z_a^{inod} and reflection coefficient Γ_a^{od} at port 2 can be derived as

$$Z_a^{inod} = B_a^{od} \Big/ D_a^{od} \tag{16}$$

$$\Gamma_a^{od} = \left(Z_a^{inod} - Z_b\right) \Big/ \left(Z_a^{inod} + Z_b\right) \tag{17}$$

Then, S_{22}, S_{32} and S_{33} can be in general deduced as

$$S_{22} = \left(k^2\Gamma_a^{ev} + \Gamma_a^{od}\right) \Big/ \left(1+k^2\right) \tag{18a}$$

$$S_{32} = k\left(\Gamma_b^{ev} - \Gamma_a^{od}\right) \Big/ \left(1+k^2\right) \tag{18b}$$

$$S_{33} = \left(k^2\Gamma_b^{od} + \Gamma_b^{ev}\right) \Big/ \left(1+k^2\right) \tag{18c}$$

Finally, the *i*-th isolation resistor R_i can be calculated by $R_i = R_{ia} + R_{ib}$.

C. THE GENERAL RESPONSE OF PROPOSED WPD

A schematic of general *S*-parameters is shown in Fig. 4. In this work, the proposed WPD could not only provide

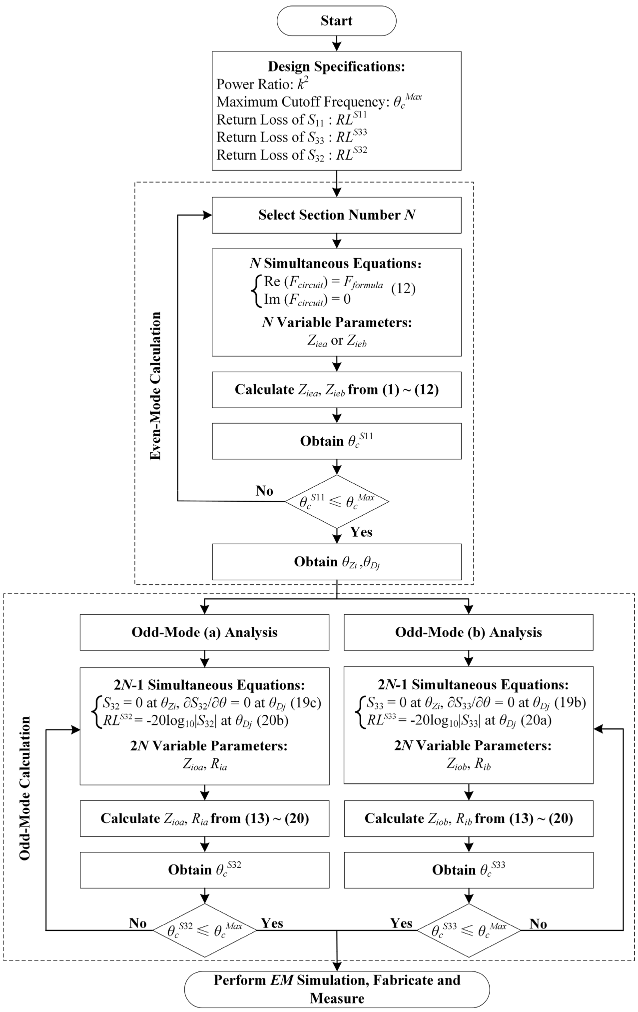

FIGURE 5. Design flowchart for the proposed WPD.

TABLE 1. Different section number of UWB WPD, where design condition: $k^2 = 2$, $Z_a = 50\ \Omega$, $1/(1/Z_b + 1/Z_c) = 25\ \Omega$, $Z_{Nea}/Z_{Noa} = Z_{Neb}/Z_{Nob} = 11/9$, $RL^{S11} = RL^{S32} = RL^{S33} = 20$ dB.

Selected Examples		Example A	Example B	Example C	Example D
Section Number N		$N = 2$	$N = 3$	$N = 4$	$N = 5$
Characteristic Impedances (Ω)	Z_{1ea}	59.9813	62.7896	64.1781	64.9843
	Z_{1eb}	119.9627	125.5791	128.3563	129.9686
	Z_{1oa}	35.1380	28.1086	24.1401	21.7732
	Z_{1ob}	38.3642	29.0670	25.1671	22.9421
	Z_{2ea}	46.8896	53.0330	56.7436	59.0777
	Z_{2eb}	93.7792	106.0660	113.4873	118.1554
	Z_{2oa}	37.7006	42.3001	39.8489,	36.1788
	Z_{2ob}	76.7284	55.5731	45.0454	38.7014
	Z_{3ea}		44.7925	49.5650	53.0330
	Z_{3eb}		89.5850	99.1301	106.0660
	Z_{3oa}		36.6484	40.7124	41.9136
	Z_{3ob}		73.2968	62.1468	53.7426
	Z_{4ea}			43.8233	47.6068
	Z_{4eb}			87.6467	95.2136
	Z_{4oa}			35.8555	38.6560
	Z_{4ob}			71.7109	64.6240
	Z_{5ea}				43.2797
	Z_{5eb}				86.5594
	Z_{5oa}				35.4107
	Z_{5ob}				70.8213
Isolation Resistors (Ω)	R_1	99.7815	88.7466	87.1499	88.6157
	R_2	203.4381	187.0098	171.6078	166.8784
	R_3		312.0947	281.6100	253.7770
	R_4			415.5174	389.6781
	R_5				510.7434
Cutoff Frequency (°)	θ_c^{S11}	48.24	34.56	26.64	21.59
	θ_c^{S32}	49.05	35.12	26.82	21.96
	θ_c^{S33}	46.80	34.33	26.55	21.75

Chebyshev equal-ripple responses of S_{11}, S_{21} and S_{31}, but also maintain non-Chebyshev equal-ripple responses of S_{32} and S_{33}.

From Fig. 4, S_{11}, S_{33} and S_{32} provide N reflection (or isolation) zeros and $N-1$ deviation zeros in a single period. Their definitions are given as

$$S_{11}|_{\theta=\theta_{Zi}} = 0 \quad \text{and} \quad \frac{\partial S_{11}}{\partial\theta}|_{\theta=\theta_{Dj}} = 0 \tag{19a}$$

$$S_{33}|_{\theta=\theta_{Zi}} = 0 \quad \text{and} \quad \frac{\partial S_{33}}{\partial\theta}|_{\theta=\theta_{Dj}} = 0 \tag{19b}$$

$$S_{32}|_{\theta=\theta_{Zi}} = 0 \quad \text{and} \quad \frac{\partial S_{32}}{\partial\theta}|_{\theta=\theta_{Dj}} = 0 \tag{19c}$$

where $i = 1, 2, \ldots, N; j = 1, 2, \ldots, N-1$.

RL^{S11} is the return loss of S_{11} at θ_{Dj}. Similarly, RL^{S33} and RL^{S32} are the return losses of S_{33} and S_{32} at θ_{Dj}, respectively, where RL^{S11}, RL^{S33} and RL^{S32} can be selected arbitrarily. In order to realize equal-ripple responses of S_{33} and S_{32}, the following equations should be maintained.

$$RL^{S33} = 20\log_{10}|S_{33}||_{\theta=\theta_{Dj}} \tag{20a}$$

$$RL^{S32} = 20\log_{10}|S_{32}||_{\theta=\theta_{Dj}} \tag{20b}$$

Similarly, θ_c^{S32} and θ_c^{S33} are defined as the electrical lengths at the lower cutoff frequencies of S_{33} and S_{32}, respectively. Although these three electrical lengths are naturally different, the difference among them is usually very small.

D. PROPOSED ALGORITHM

To clarify the design method of proposed WPD, its detailed algorithm is summarized as a flowchart in Fig. 5. In the following, a few critical design steps are further described.

Step 1: Specify the desired power ratio k^2, maximum cutoff frequency θ_c^{Max} (where, $[\theta_c^{S11}, \theta_c^{S33}, \theta_c^{S32}]_{Max} \leq \theta_c^{Max}$), and the return loss of S_{11}, S_{33} and S_{32}: RL^{S11}, RL^{S33} and RL^{S32}.

Step 2: Even-mode calculation

(i) Based on the specifications given above, choose a suitable section number N

(ii) When N is determined, the number of simultaneous equations and variable parameters are equal to N. Based on

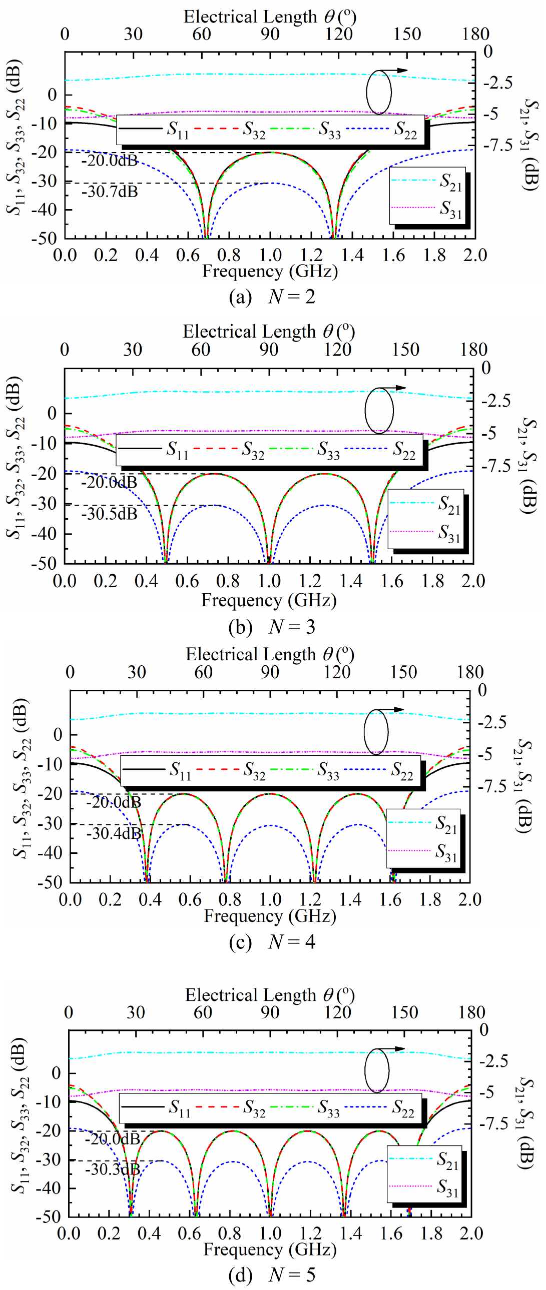

FIGURE 6. **Circuit simulation results based on Table 1 for the proposed topology of UWB WPD with different section numbers.**

the constraints of simultaneous equations in (12), the single unique solution of all characteristic impedances (Z_{iea} and Z_{ieb}, where $i = 1, 2, \ldots, N$) can be calculated from (1)-(12).

(iii) Then, θ_c^{S11} can be calculated. If $\theta_c^{S11} > \theta_c^{Max}$, go back to step 2 (i), and choose different N. If $\theta_c^{S11} \leq \theta_c^{Max}$, θ_{Zi} and θ_{Di} are determined automatically. These parameters will be used to evaluate the equal-ripple conditions in odd-mode calculation.

Step 3: Odd-mode (a) calculation

(i) In order to make sure that S_{32} has its equal-ripple response with fixed return loss (RL^{S32}), suitable Z_{ioa} and R_{ia} will be calculated in odd-mode (a) analysis.

TABLE 2. **Different power ratio of UWB 3-section WPD, where design condition: $Z_a = 50\ \Omega$, $1/(1/Z_b + 1/Z_c) = 25\ \Omega$, $Z_{3ea}/Z_{3oa} = Z_{3eb}/Z_{3ob} = 11/9$, $RL^{S11} = RL^{S32} = 20$ dB.**

Selected Examples		Example E	Example F	Example G
Power ratio		$k^2 = 1.0$	$k^2 = 1.5$	$k^2 = 2.5$
Characteristic Impedances (Ω)	Z_{1ea}	83.7194	69.7662	58.6036
	Z_{1eb}		104.6493	146.5090
	Z_{1oa}	42.8615	34.0654	23.9149
	Z_{1ob}		20.6266	38.0614
	Z_{2ea}	70.7107	58.9256	49.4975
	Z_{2eb}		88.3883	123.7437
	Z_{2oa}	61.6190	49.7661	37.1592
	Z_{2ob}		42.0451	69.7452
	Z_{3ea}	59.7233	49.7694	41.8063
	Z_{3eb}		74.6541	104.5158
Isolation Resistors (Ω)	R_1	100.4545	84.8417	95.7451
	R_2	140.6128	178.1376	199.6215
	R_3	421.5813	294.5903	339.8687
Cutoff Frequency (°)	θ_c^{S11}	34.56	34.56	34.56
	θ_c^{S32}	35.14	35.13	35.10
	θ_c^{S33}	40.20	33.18	34.84

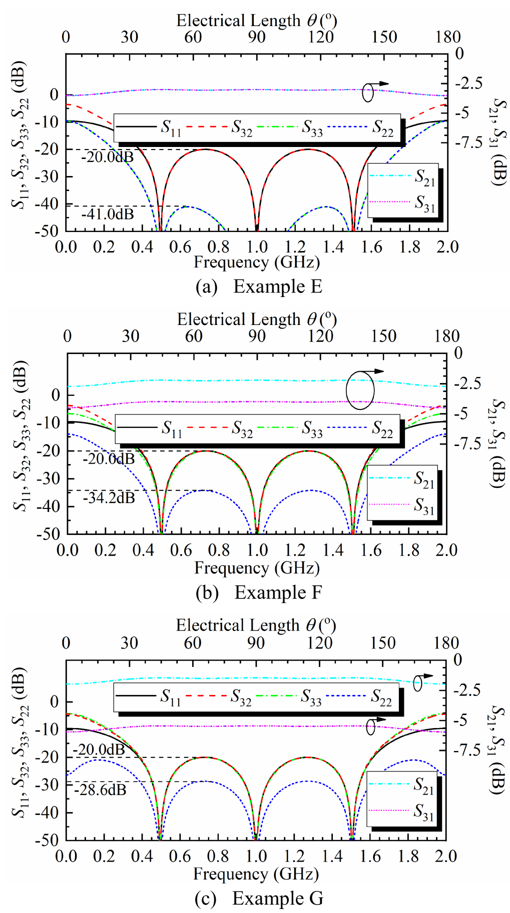

FIGURE 7. **Circuit simulation results based on Table 2 for the proposed topology of 3-section WPD with different power ratios.**

(ii) There are $2N - 1$ constraints and $2N$ variable parameters (Z_{ioa} and R_{ia}) in simultaneous equations (19c) and (20b).

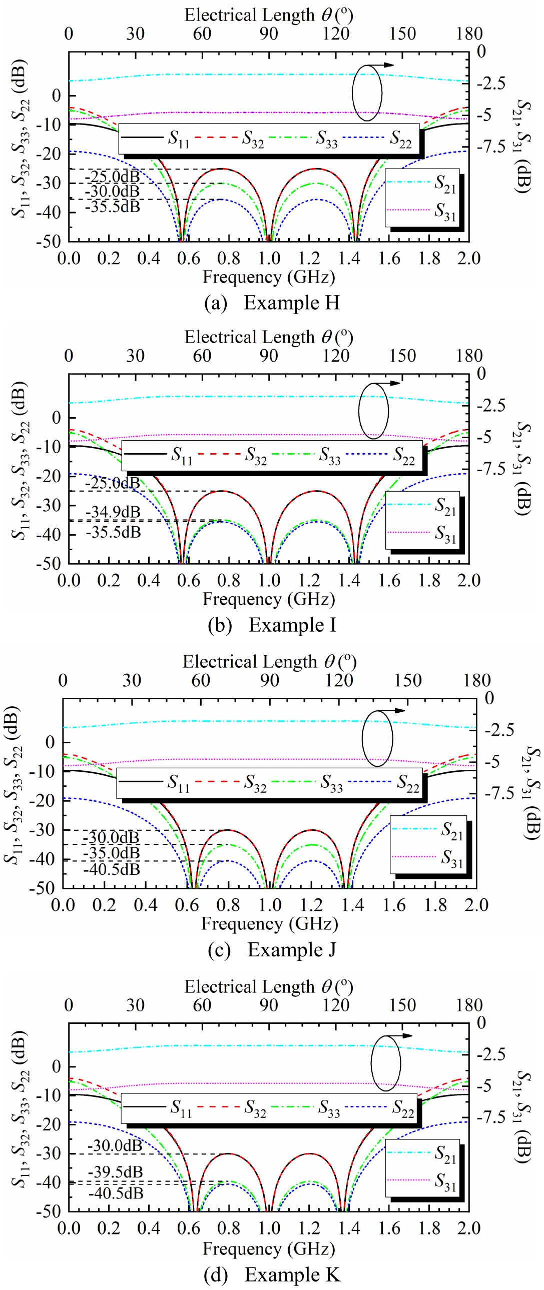

FIGURE 8. Circuit simulation results based on Table 3 for the proposed topology of 3-section WPD with different return losses.

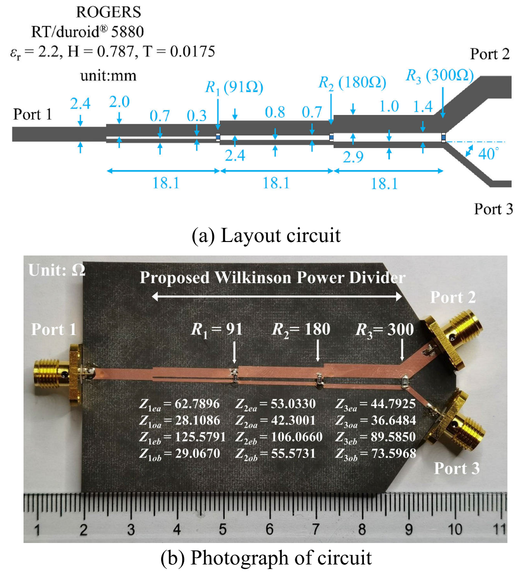

FIGURE 9. Experimental circuit of proposed WPD (Example B).

Therefore, Z_{ioa} and R_{ia} can be directly calculated from (13)-(20) with one degree of freedom.

(iii) Then, θ_c^{S32} can be calculated. If $\theta_c^{S32} > \theta_c^{Max}$, go back to step 3 (ii), and choose a different value from degree of freedom. If $\theta_c^{S32} \leq \theta_c^{Max}$, all the Z_{ioa} and R_{ia} will be finally determined.

Step 4: Odd-mode (b) calculation

Similarly to step 3, Z_{iob} and R_{ib} will be calculated to make sure that S_{33} has its equal-ripple response with fixed return loss (RL^{S33}). Finally, isolation resistor R_i can be calculated by $R_i = R_{ia} + R_{ib}$. Due to the limited pages, detailed process is omitted.

Step 5: Verification

Perform EM simulation and slightly adjust the physical dimensions towards optimized target if necessary.

III. DESIGN EXAMPLES

For the proposed topology in Fig. 1 (b), by using the flowchart in Fig. 5, the general response in Fig. 4 will be evidently validated in this section. Under the condition of $Z_a = 50\ \Omega$ and $Z_bZ_c/(Z_b + Z_c) = 25\ \Omega$, several design examples and circuit simulation results are given for discussion.

A. DISCUSSION OF SECTION NUMBER (N)

For different section numbers (N), four design examples ($N = 2$ in Example A, $N = 3$ in Example B, $N = 4$ in Example C and $N = 5$ in Example D) are tabulated in Table 1 under the conditions of fixed power ratio $k^2 = 2$, fixed terminal loads ($Z_a = 50\ \Omega$ and $1/(1/Z_b + 1/Z_c) = 25\ \Omega$), fixed coupling strengths ($Z_{Nea}/Z_{Noa} = Z_{Neb}/Z_{Nob} = 11/9$) and fixed equal-ripple levels ($RL^{S11} = RL^{S32} = RL^{S33} = 20$ dB).

Their circuit simulation results are shown in Fig. 6 for verification. By selecting different N, the ripple level of S_{11}, S_{32} and S_{33} can be controlled at -20 dB very well, while keeping the ripple level of S_{22} is around -30 dB.

B. DISCUSSION OF POWER RATIO (k^2)

For different power ratios (k^2), three design examples ($k^2 = 1.0$ in Example E, $k^2 = 1.5$ in Example F and $k^2 = 2.5$ in Example G) are tabulated in Table 2 under the conditions of fixed section number $N = 3$, fixed terminal loads ($Z_a = 50\ \Omega$ and $1/(1/Z_b + 1/Z_c) = 25\ \Omega$), fixed coupling strengths ($Z_{3ea}/Z_{3oa} = Z_{3eb}/Z_{3ob} = 11/9$) and fixed equal-ripple levels ($RL^{S11} = RL^{S32} = 20$ dB). Their circuit simulation results are shown in Fig. 7. Compared with

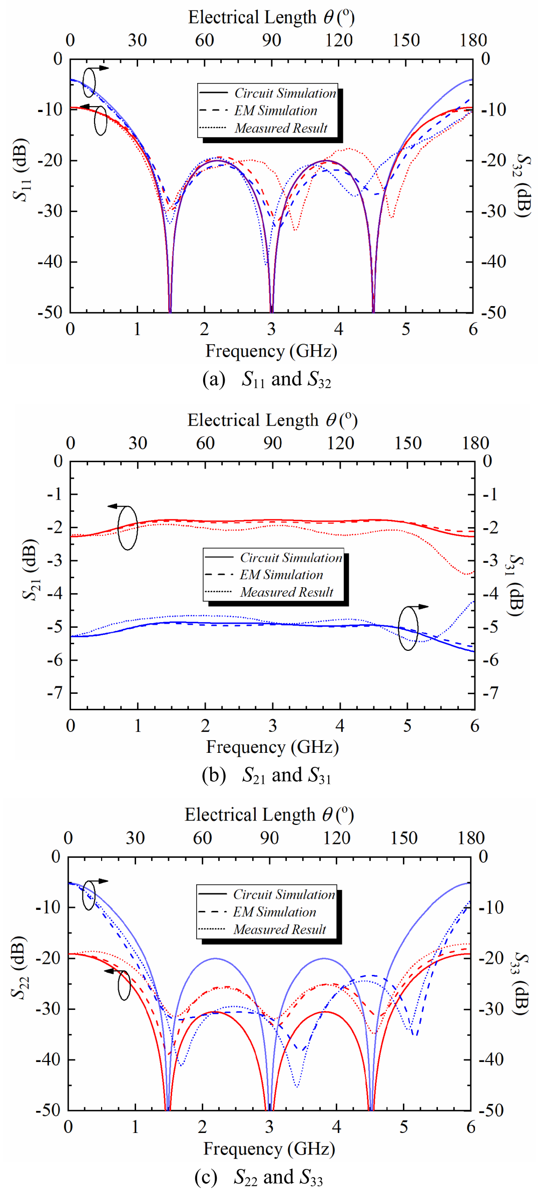

FIGURE 10. Circuit simulation, EM simulation and measured results of proposed WPD (Example B).

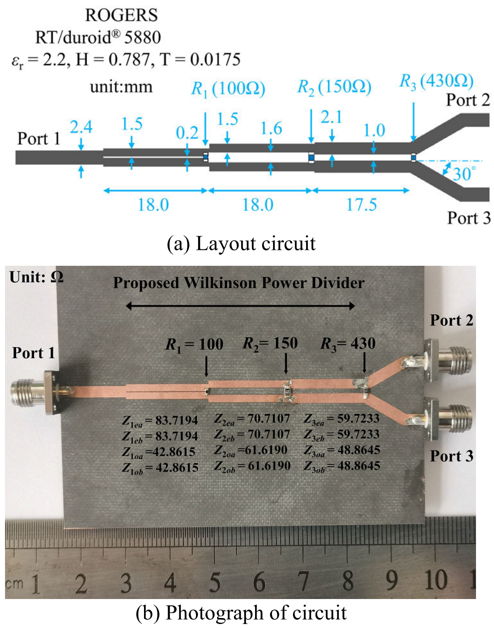

FIGURE 11. Experimental circuit of proposed WPD (Example E).

TABLE 3. Different ripple levels of S_{11} S_{32} and S_{33} in UWB 3-section WPD, where design condition: $k^2 = 2$, $Z_a = 50\ \Omega$, $1/(1/Z_b + 1/Z_c) = 25\ \Omega$, $Z_{3ea}/Z_{3oa} = Z_{3eb}/Z_{3ob} = 11/9$.

Selected Examples		Example H	Example I	Example J	Example K
$RL^{S11} = RL^{S32}$		25.0 dB		30.0 dB	
RL^{S33}		30.0 dB	34.9 dB	35.0 dB	39.5 dB
Characteristic Impedances (Ω)	Z_{1ea}	64.9097	64.9097	66.2445	66.2445
	Z_{1eb}	129.8194	129.8194	132.4890	132.4890
	Z_{1oa}	24.1738	24.1738	21.6244	21.6244
	Z_{1ob}	38.4461	55.7349	33.9625	47.8972
	Z_{2ea}	53.0330	53.0330	53.0330	53.0330
	Z_{2eb}	106.0660	106.0660	106.0660	106.0660
	Z_{2oa}	42.8247	42.8247	43.5598	43.5598
	Z_{2ob}	76.1863	105.7434	77.3176	105.7830
	Z_{3ea}	43.3294	43.3294	42.4563	42.4563
	Z_{3eb}	86.6589	86.6589	84.9127	84.9127
Isolation Resistors (Ω)	R_1	78.2685	96.3832	67.0266	82.2682
	R_2	145.0567	136.1601	133.897	127.4825
	R_3	567.2133	731.4264	806.3097	1076.205
Cutoff Frequency (°)	θ_c^{S11}	43.35	43.35	50.88	50.88
	θ_c^{S32}	43.59	43.59	50.99	50.99
	θ_c^{S33}	44.12	44.70	51.25	51.51

equal power ratio case (Example E), there is a sufficient degree of freedom to control $RL^{S33} = 20$ dB for unequal power ratio cases. In other words, three ripple levels (S_{11}, S_{32} and S_{33}) can only be controlled for unequal power ratio case, unfortunately, one of these three ripple levels cannot be controlled for equal power ratio. By selecting a larger power ratio, the ripple level of S_{22} can be increased from −41.0 dB to −28.6 dB, with the bandwidths of θ_c^{S11}, θ_c^{S32} and θ_c^{S33} to be almost unchanged.

C. DISCUSSION OF RETURN LOSS (RL^{S11}, RL^{S32} & RL^{S33})

Even though the section number and power ratio are all determined, different return losses also can be selected. Four design examples (Example H, I, J and K) are tabulated in Table 3 under the conditions of fixed terminal loads ($Z_a = 50\ \Omega$ and $1/(1/Z_b + 1/Z_c) = 25\ \Omega$), fixed coupling strengths ($Z_{3ea}/Z_{3oa} = Z_{3eb}/Z_{3ob} = 11/9$) and fixed power ratio ($k^2 = 2$).

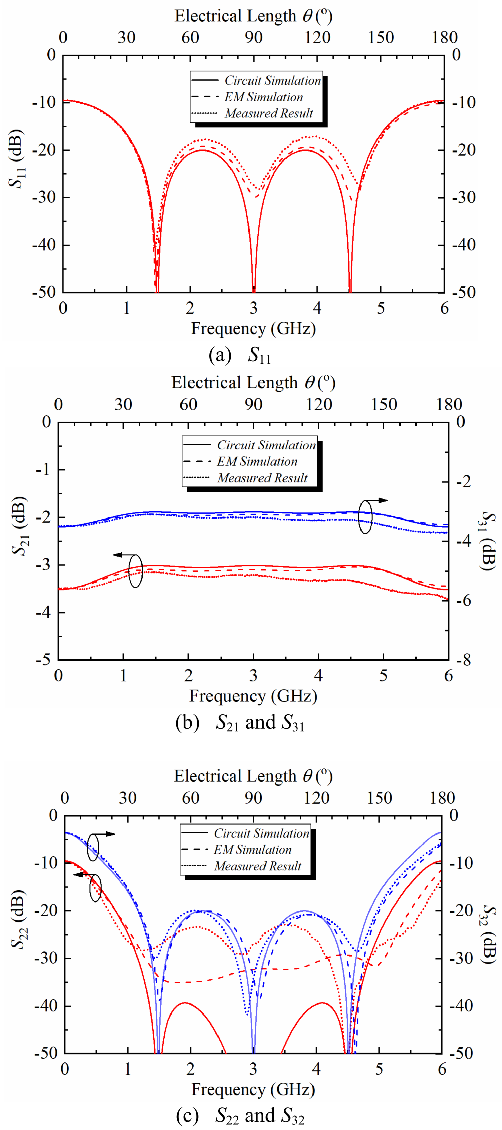

(a) S_{11}

(b) S_{21} and S_{31}

(c) S_{22} and S_{32}

FIGURE 12. Circuit simulation, EM simulation and measured results of proposed WPD (Example E).

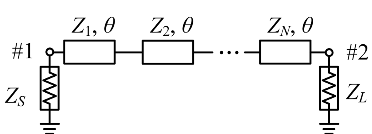

FIGURE 13. The general topology of N-section TLT.

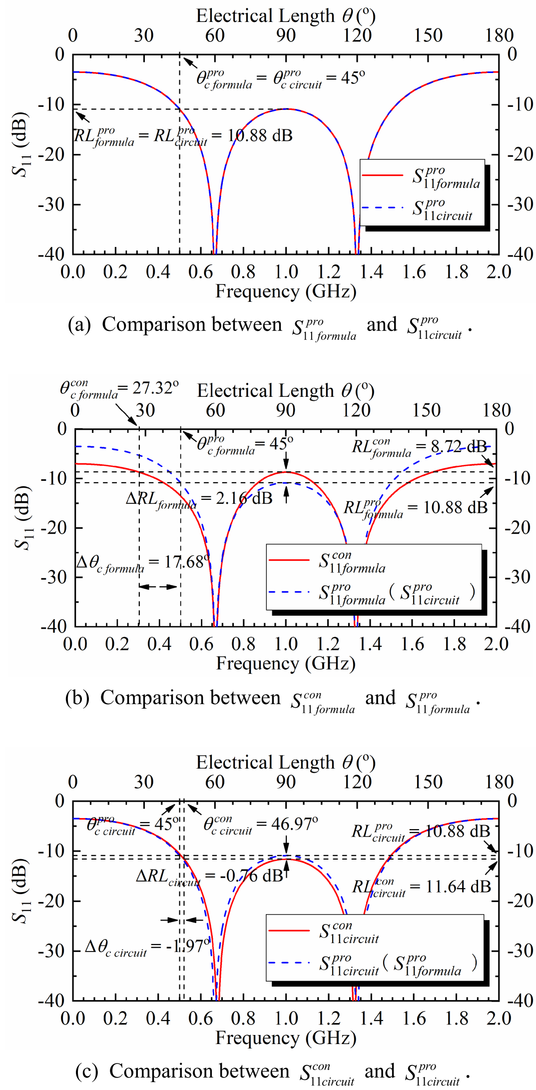

(a) Comparison between $S_{11formula}^{pro}$ and $S_{11circuit}^{pro}$.

(b) Comparison between $S_{11formula}^{con}$ and $S_{11formula}^{pro}$.

(c) Comparison between $S_{11circuit}^{con}$ and $S_{11circuit}^{pro}$.

FIGURE 14. S-parameter comparison under the conditions of $Z_S = 150\ \Omega$, $Z_L = 30\ \Omega$, $N = 2$, $\theta_C = 45°$.

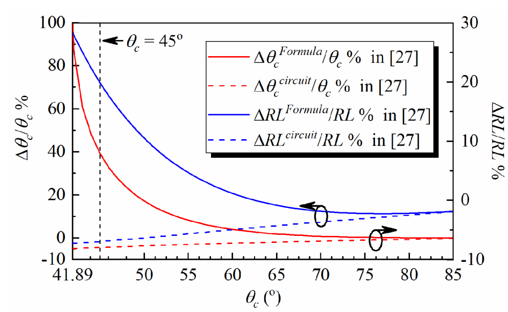

FIGURE 15. The delta error of return loss and bandwidth under different cutoff frequencies (θ_C).

Their circuit simulation results are shown in Fig. 8. From these four examples, it can be figure out that: when $RL^{S11} = RL^{S32} = 25.0$ dB, RL^{S33} can be designed from 30.0 dB to 34.9 dB; $RL^{S11} = RL^{S32} = 30.0$ dB, RL^{S33} can be designed from 35.0 dB to 39.5 dB. If Z_{3ea}/Z_{3oa} and Z_{3eb}/Z_{3ob} could be selected arbitrarily, the designable range of RL^{S33} can be further widened.

IV. EXPERIMENTS AND RESULTS

In the experiment, two circuits (Example B and Example E) are selected for fabrication on Rogers RT/duroid 5880 substrate, where dielectric constant $\varepsilon_r = 2.2$, $\tan\delta = 0.0009$ and

TABLE 4. Comparison of several recent ultra-wideband WPDs.

Ref.	UPR	IL (dB)	FBW (%) / RL (dB) / Equal ripple or not / Controllable ripple level or not				Size ($\lambda_g \times \lambda_g$)
			RL^{S11}	RL^{S22}	RL^{S32}	RL^{S33}	
[3]	No	0.4	94.9% / 10 dB / No / No	83.2% / 10 dB / No / No	- / 10 dB / No / No	83.2% / 10 dB / No / No	0.5×1.0
[4]	No	0.2	62.0% / 15 dB / No / No	- / 15 dB / No / No	- / 20 dB / No / No	- / 15 dB / No / No	0.72×0.39
[5]	No	0.6	54.0% / 10 dB / No / No	48.6% / 10 dB / No / No	127.0% / 14 dB / No / No	48.6% / 10 dB / No / No	0.63×0.37
[6]	No	0.7	78.0% / 10 dB / No / No	- / - / No / No	78.0% / 17.5 dB / No / No	- / - /No / No	0.74×0.31
[11]	No	0.66	104.5% / 15 dB / No /No	- / 15 dB / No / No	- / 15 dB / No / No	- / 15 dB / No / No	0.2×0.15
[13]	No	0.47	103.0% / 20 dB / No / No	120.0% / 20dB / No / No	116.0% / 20 dB / No / No	120.0% / 20 dB / No / No	0.55×0.1
[16]	No	1.6	62.1% / 10 dB / No / No	63.0% / 10 dB / No / No	- / 10 dB / No / No	63.0% / 10 dB / No / No	-
[17]	No	2.0	100.7% / 10 dB / No / No	116.8% / 10dB / No / No	156.2% / 10 dB / No / No	116.8% / 10 dB / No / No	1×0.75
[22]*	No	0.5	107.3% /17.8dB /Yes/No	113.3%/ < 20dB / No/No	109.7%/ 19.8 dB / No / No	113.3% / < 20 dB / No / No	1.25×0.5
[29]*	Yes	0.2	111.8%/19.1dB/ Yes/ No	- / 19.1 dB / No / No	- / 23 dB / No / No	- / 19.1 dB / No / No	-
		0.2	82.4% /17.7dB/ Yes / No	- / 17.7 dB / No / No	- / 20 dB / No / No	- / 17.7 dB / No / No	-
[30]*	Yes	0.5	110.0% /15 dB / Yes / No	- / 15 dB / No / No	- / 20 dB / No / No	- / 15 dB / No / No	0.64×0.24
		0.8	140.0% /15 dB / Yes / No	- / 15 dB / No / No	- / 20 dB / No / No	- / 15 dB / No / No	0.92×0.35
[31]	Yes	2.0	- / - /No / No	- / - /No / No	- / 20 dB / No / No	- / - / No / No	0.99×0.3
		0.8	- / - /No / No	- / - /No / No	- / 25 dB / No / No	- / - / No / No	0.85×0.4
This work #	**No**	**0.3**	**132.5% / 17.2dB / Yes/ Yes**	**158.2% / 22.8dB / Yes/ Yes**	**123.7% / 20.8dB /Yes / Yes**	**158.2% / 22.8dB / Yes/ Yes**	**0.73×0.07**
This work #	**Yes**	**0.3**	**139.4% / 18.0dB / Yes/ Yes**	**124.1% / 25.1dB / Yes/ Yes**	**120.0% / 19.5dB /Yes / Yes**	**145.3% / 24.4dB /Yes / Yes**	**0.74×0.07**

UPR: unequal power ratio; IL: insertion loss; FBW: fractional bandwidth; RL: return loss.

* S_{11} is approximate first kind Chebyshev transfer function by Hansen's approximation. # S_{11} fits the first kind Chebyshev transfer function.

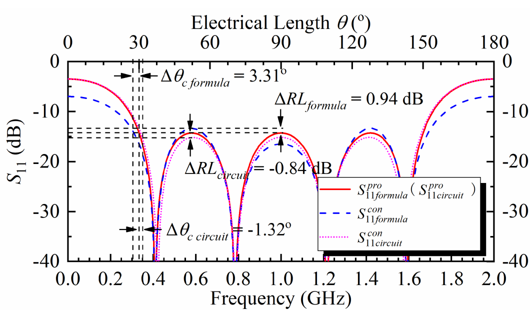

FIGURE 16. ***S*-parameter comparison under the conditions of $Z_S = 150\ \Omega$, $Z_L = 30\ \Omega$, $N = 4$, $\theta_c = 30°$.**

thickness h = 0.787 mm. The layout and photograph of Example B is shown in Fig. 9. The circuit simulation, *EM* simulation (Sonnet) and measurements are shown in Fig. 10. The S-matrix parameters of this circuit are directly measured using the MS46122B vector network analyzer with the load impedances to be all equal to 50 Ω. Then, they are recalculated with reference to different actual loaded impedances at all the three ports (Z_a, Z_b and Z_c).

Similarly, the layout and photograph of Example E is shown in Fig. 11. The circuit simulation, *EM* simulation (Sonnet) and measurements are shown in Fig. 12. For both cases of our experiments, simulated and measured results are matched very well.

Finally, our detailed comparisons with several previous works are listed in Table 4 in terms of different parameters and overall size. By using the proposed synthesis method the presented wideband WPD topology could indeed achieve in-band equal-ripple performance and controllable ripple levels at the same time.

V. CONCLUSION

A novel synthesis method for design of multi-section UWB WPDs is proposed in this paper. By using the ACLSs, arbitrary power ratio can be realized with compact circuit size. The novelties of proposed synthesis method have been demonstrated and verified through several design examples. Our theoretical work has well revealed that all the *S*-parameters (S_{11}, S_{21}, S_{31}, S_{22}, S_{33} and S_{32}) of proposed WPD can be effectively designed with equal-ripple performance and controllable ripple levels. Finally, two WPD circuit prototypes with $N = 3$ are fabricated and tested, and the measured results are found in good agreement with the simulated ones, thus validating the effectiveness of the proposed synthesis method very well.

APPENDIX

In this appendix, a general topology of N-section TLT is shown in Fig. 13. In order to distinguish the differences between the proposed work and Cohn's work [27] in details, three aspects are compared and discussed as follows.

A. COMPARISON OF THEORETICAL TRANSFER FUNCTION

From (9)-(11) in this paper, the theoretical transfer function of proposed work $S_{21formula}^{pro}$ can be written as

$$\left|S_{21formula}^{pro}(\theta)\right| = \frac{1}{\sqrt{1+\varepsilon^2\left|T_N(\cos\theta/\cos\theta_c)\right|^2}} \quad \text{(A1)}$$

where $\varepsilon = \left[\left(1+k^2\right)Z_a - k^2Z_b\right]/\left[2k\cdot T_N\left(1/\cos\theta_c\right)\sqrt{\left(1+k^2\right)Z_aZ_b}\right]$, $T_N(x)$ is the Chebyshev polynomial of the first kind, θ_c is the electrical length at lower cutoff frequency.

However, from (2) in [27], VSWR design method is used to derive broadband response. Then, the theoretical transfer function of Cohn's work $S_{21formula}^{con}$ can be written as

$$\left|S_{21formula}^{con}(\theta)\right| = \frac{2\sqrt{1+\ln\left(Z_L/Z_S\right)\frac{T_N(\cos\theta/\cos\theta_c)}{T_N(1/\cos\theta_c)}}}{2+\ln\left(Z_L/Z_S\right)\frac{T_N(\cos\theta/\cos\theta_c)}{T_N(1/\cos\theta_c)}} \quad \text{(A2)}$$

Because $\left|S_{21formula}^{pro}(\theta)\right| \neq \left|S_{21formula}^{con}(\theta)\right|$, the proposed method and VSWR method [27] are a different technique for TLT to derive equal-ripple response.

B. CALCULATION OF CHARACTERISTIC IMPEDANCES

From (8)-(12) in this paper, the characteristic impedances can be calculated from the following simultaneous equations

$$\begin{cases} \mathrm{Re}\left(F_{circuit}^{pro}\right) = F_{formula}^{pro} \\ \mathrm{Im}\left(F_{circuit}^{pro}\right) = 0 \end{cases}$$
$$\Rightarrow \begin{cases} F_{circuit}^{pro} = \varepsilon\cdot T_N\left(\cos\theta/\cos\theta_c^{S11}\right) \\ B_T - Z_SZ_LC_T = 0 \end{cases} \quad \text{(A3)}$$

where, A_T, B_T, C_T and D_T are four elements of the total *ABCD* matrix of the TLT.

However, from (13) in [27], the characteristic impedances can be calculated from the following simultaneous equations

$$\ln\frac{Z_1}{Z_S} : \ln\frac{Z_2}{Z_1} : \cdots : \ln\frac{Z_L}{Z_N} = a_1 : a_2 : \cdots : a_N \quad \text{(A4)}$$

where $a_n = \frac{1}{2}\ln\frac{Z_{n+1}}{Z_n}$, $1 \leq n \leq N$.

Therefore, the calculation methods between this work and Cohn's work [27] are quite different.

C. THE COMPARISON OF DELTA ERROR

Two 150 Ω – 30 Ω TLTs examples ($N = 2$ and $N = 4$) are shown in this section. Compared with VSWR design method and its Hansen's approximation in Cohn's work [27], the first-kind Chebyshev equal-ripple performance (S_{11} and S_{21}) can be exactly realized by virtue of the cascaded TLT in this work.

1) CASE OF $N = 2$

As for the passband, the differences of return loss and bandwidth between them can be presented more clearly in S_{11} than S_{21}. Fig. 14 shows the detailed differences of S_{11} for this work and Cohn's work [27] under the condition of $\theta_c = 45°$. In Fig. 14 (a), $S_{11formula}^{pro}$ and $S_{11circuit}^{pro}$ are overlapped, where $RL_{formula}^{pro}(\theta = 90°) = RL_{formula}^{pro}(\theta = 45°) = 10.88$ dB and $\theta_{c\,formula}^{pro} = \theta_c = 45°$. Therefore, there is no delta error in the proposed work.

In Fig. 14 (b), $S_{11formula}^{con}$ and $S_{11formula}^{pro}$ are quite different, where, $RL_{formula}^{con}(\theta = 90°) = 8.72$ dB and $\theta_{c\,formula}^{con} = 27.32°$. The delta error of return loss and bandwidth are equal to $\Delta RL_{formula} = RL_{formula}^{pro}(\theta = 90°) - RL_{formula}^{con}(\theta = 90°) = 2.16$ dB and $\Delta\theta_{c\,formula} = \theta_{c\,formula}^{pro} - \theta_{c\,formula}^{con} = 17.68°$, respectively.

In Fig. 14 (c), $S_{11circuit}^{con}$ and $S_{11circuit}^{pro}$ are also different. The delta error of return loss and bandwidth are $\Delta RL_{circuit} = -0.76$ dB and $\Delta\theta_{c\,circuit} = -1.97°$, respectively.

Finally, for different θ_c, the delta error of return loss and bandwidth are calculated in Fig. 15. Compared with Cohn's work in [27], the proposed design method has no delta error of return loss and bandwidth at all, so as to prove its advantageous features against other existing ones.

2) CASE OF $N = 4$

Fig. 16 shows the S_{11} under the condition of $\theta_c = 30°$. As N increases, there is also no delta error again in the proposed work. However, equal-ripple level cannot be realized by the Cohn's method [27], where the delta errors of return loss and bandwidth are equal to $\Delta RL_{formula} = 0.94$ dB, $\Delta RL_{circuit} = -0.84$ dB and $\Delta\theta_{c\,formula} = -1.32°$, $\Delta\theta_{c\,circuit} = 3.31°$, respectively.

REFERENCES

[1] E. J. Wilkinson, "An N-way hybrid power divider," *IEEE Trans. Microw. Theory Techn.*, vol. MTT-8, no. 1, pp. 116–118, Jan. 1960.
[2] L. Chiu, T. Y. Yum, Q. Xue, and C. H. Chan, "A wideband compact parallel-strip 180/spl deg/ Wilkinson power divider for push-pull circuitries," *IEEE Microw. Wireless Compon. Lett.*, vol. 16, no. 1, pp. 49–51, Jan. 2006.
[3] S. W. Wong and L. Zhu, "Ultra-wideband power divider with good in-band splitting and isolation performances," *IEEE Microw. Wireless Compon. Lett.*, vol. 18, no. 8, pp. 518–520, Aug. 2008.
[4] M. A. Maktoomi, M. S. Hashmi, and F. M. Ghannouchi, "Theory and design of a novel wideband DC isolated Wilkinson power divider," *IEEE Microw. Wireless Compon. Lett.*, vol. 26, no. 8, pp. 586–588, Aug. 2016.
[5] D. Chen, L. Zhu, and C. Cheng, "Dual-resonant-mode (DRM) impedance transformer and its application to wideband 3 dB power divider," *IEEE Microw. Wireless Compon. Lett.*, vol. 23, no. 9, pp. 471–473, Sep. 2013.
[6] Y. Liu, L. Zhu, and S. Sun, "Proposal and design of a power divider with wideband power division and port-to-port isolation: A new topology," *IEEE Trans. Microw. Theory Techn.*, vol. 68, no. 4, pp. 1431–1438, Apr. 2020.
[7] H. Oraizi and M. S. Esfahlan, "Miniaturization of Wilkinson power dividers by using defected ground structures," *Prog. Electromagn. Res. Lett.*, vol. 4, pp. 113–120, 2008.
[8] X. Lan, P. Chang-Chien, F. Fong, D. Eaves, X. Zeng, and M. Kintis, "Ultra-wideband power divider using multi-wafer packaging technology," *IEEE Microw. Wireless Compon. Lett.*, vol. 21, no. 1, pp. 46–48, Jan. 2011.

[9] Y. Lin and J. Lee, "Miniature ultra-wideband power divider using bridged T-coils," *IEEE Microw. Wireless Compon. Lett.*, vol. 22, no. 8, pp. 391–393, Aug. 2012.
[10] K. Kim and C. Nguyen, "An ultra-wideband low-loss millimeter-wave slow-wave Wilkinson power divider on 0.18μm SiGe BiCMOS process," *IEEE Microw. Wireless Compon. Lett.*, vol. 25, no. 5, pp. 331–333, May 2015.
[11] C. Tang and J. Chen, "A design of 3-dB wideband microstrip power divider with an ultra-wide isolated frequency band," *IEEE Trans. Microw. Theory Techn.*, vol. 64, no. 6, pp. 1806–1811, Jun. 2016.
[12] I. Ju, M. Cho, I. Song, and J. D. Cressler, "A compact, wideband lumped-element Wilkinson power divider/combiner using symmetric inductors with embedded capacitors," *IEEE Microw. Wireless Compon. Lett.*, vol. 26, no. 8, pp. 595–597, Aug. 2016.
[13] T. Yu, "A broadband Wilkinson power divider based on the segmented structure," *IEEE Trans. Microw. Theory Techn.*, vol. 66, no. 4, pp. 1902–1911, Apr. 2018.
[14] H. Zhu, Z. Cheng, and Y. J. Guo, "Design of wideband in-phase and out-of-phase power dividers using microstrip-to-slotline transitions and slotline resonators," *IEEE Trans. Microw. Theory Techn.*, vol. 67, no. 4, pp. 1412–1424, Apr. 2019.
[15] A. M. Abbosh, "Design of ultra-wideband three-way arbitrary power dividers," *IEEE Trans. Microw. Theory Techn.*, vol. 56, no. 1, pp. 194–201, Jan. 2008.
[16] S. S. Gao, S. Sun, and S. Xiao, "A novel wideband bandpass power divider with harmonic-suppressed ring resonator," *IEEE Microw. Wireless Compon. Lett.*, vol. 23, no. 3, pp. 119–121, Mar. 2013.
[17] K. Song and Q. Xue, "Novel ultra-wideband (UWB) multilayer slotline power divider with bandpass response," *IEEE Microw. Wireless Compon. Lett.*, vol. 20, no. 1, pp. 13–15, Jan. 2010.
[18] L. Jiao, Y. Wu, Y. Liu, Q. Xue, and Z. Ghassemlooy, "Wideband filtering power divider with embedded transversal signal-interference sections," *IEEE Microw. Wireless Compon. Lett.*, vol. 27, no. 12, pp. 1068–1070, Dec. 2017.
[19] M. Chen and C. Tang, "Design of the filtering power divider with a wide passband and stopband," *IEEE Microw. Wireless Compon. Lett.*, vol. 28, no. 7, pp. 570–572, Jul. 2018.
[20] X. Yu and S. Sun, "A novel wideband filtering power divider with embedding three-line coupled structures," *IEEE Access*, vol. 6, pp. 41280–41290, 2018.
[21] K. D. Xu, Y. Bai, X. Ren, and Q. Xue, "Broadband filtering power dividers using simple three-line coupled structures," *IEEE Trans. Compon., Packag., Manuf. Technol.*, vol. 9, no. 6, pp. 1103–1110, Jun. 2019.
[22] X. Wang, Z. Ma, T. Xie, M. Ohira, C. Chen, and G. Lu, "Synthesis theory of ultra-wideband bandpass transformer and its Wilkinson power divider application with perfect in-band reflection/isolation," *IEEE Trans. Microw. Theory Techn.*, vol. 67, no. 8, pp. 3377–3390, Aug. 2019.
[23] X. Wang, J. Wang, G. Zhang, J. Hong, and W. Wu, "Dual-wideband filtering power divider with good isolation and high selectivity," *IEEE Microw. Wireless Compon. Lett.*, vol. 27, no. 12, pp. 1071–1073, Dec. 2017.
[24] X. Wang, J. Wang, W. Choi, L. Yang, and W. Wu, "Dual-wideband filtering power divider based on coupled stepped-impedance resonators," *IEEE Microw. Wireless Compon. Lett.*, vol. 28, no. 10, pp. 873–875, Oct. 2018.
[25] C. Zhu, J. Xu, W. Kang, and W. Wu, "Microstrip multifunctional reconfigurable wideband filtering power divider with tunable center frequency, bandwidth, and power division," *IEEE Trans. Microw. Theory Techn.*, vol. 66, no. 6, pp. 2800–2813, Jun. 2018.
[26] H. Zhu, A. M. Abbosh, and L. Guo, "Planar in-phase filtering power divider with tunable power division and controllable band for wireless communication systems," *IEEE Trans. Compon., Packag., Manuf. Technol.*, vol. 8, no. 8, pp. 1458–1468, Aug. 2018.
[27] S. B. Cohn, "Optimum design of stepped transmission-line transformers," *IEEE Trans. Microw. Theory Techn.*, vol. MTT-3, no. 3, pp. 16–20, Apr. 1955.
[28] S. B. Cohn, "A class of broadband three-port TEM-mode hybrids," *IEEE Trans. Microw. Theory Techn.*, vol. MTT-16, no. 2, pp. 110–116, Feb. 1968.
[29] R. B. Ekinge, "A new method of synthesizing matched broad-band TEM-mode three-ports," *IEEE Trans. Microw. Theory Techn.*, vol. MTT-19, no. 1, pp. 81–88, Jan. 1971.
[30] M. M. Honari, L. Mirzavand, R. Mirzavand, A. Abdipour, and P. Mousavi, "Theoretical design of broadband multisection Wilkinson power dividers with arbitrary power split ratio," *IEEE Trans. Compon., Packag., Manuf. Technol.*, vol. 6, no. 4, pp. 605–612, Apr. 2016.
[31] H. Oraizi and A.-R. Sharifi, "Design and optimization of broadband asymmetrical multisection Wilkinson power divider," *IEEE Trans. Microw. Theory Techn.*, vol. 54, no. 5, pp. 2220–2231, May 2006.
[32] I. B. Kim, K. H. Kwon, S. B. Kwon, W. Mohyuddin, H. C. Choi, and K. W. Kim, "Ultra-wideband multi-section power divider on suspended stripline," in *IEEE MTT-S Int. Microw. Symp. Dig.*, Jun. 2017, pp. 427–430.
[33] Y. Wu and Y. Liu, "A unequal coupled-line Wilkinson power divider for arbitrary terminated impedances," *Prog. Electromagn. Res.*, vol. 117, pp. 181–194, 2011.
[34] S. Taravati and M. Khalaj-Amirhosseini, "Generalised single-section broad-band asymmetrical Wilkinson power divider," *IET Microw., Antennas Propag.*, vol. 6, no. 10, pp. 1164–1171, Jul. 2012.
[35] L. Zhu, S. Sun, and R. Li, *Microwave Bandpass Filters for Wideband Communications*. New York, NY, USA: Wiley, 2012.

ZIZHUO SUN (Graduate Student Member, IEEE) was born in Jilin, China, in 1997. He received the B.S. degree from the College of Electronic Science and Engineering, Jilin University, Changchun, China, in 2019, where he is currently pursuing the Ph.D. degree.

His current research interests include analysis and design of microwave passive components and microwave sensors.

XIAOLONG WANG (Member, IEEE) received the B.S. degree in communication engineering from Jilin University, Changchun, China, in 2005, the M.S. degree from the Changchun University of Science and Technology, Changchun, in 2008, and the Ph.D. degree from the University of Toyama, Toyama, Japan, in 2012.

From November 2012 to June 2013, he was a Postdoctoral Research Associate with the Art, Science and Technology Center for Cooperative Research, Kyushu University, Japan. From July 2013 to December 2015, he was a Researcher with the Plasma Research Center, University of Tsukuba, Tsukuba, Japan. Since January 2016, he has been an Assistant Professor with the Department of Electronic Engineering, Saitama University, Japan. He is currently a Professor with the College of Electronic Science and Engineering, Jilin University. His research interests include microwave/millimeter-wave system design, passive component design, and optimization techniques.

Dr. Wang is a member of the Institute of Electronics, Information and Communication Engineers (IEICE), Japan. He was a recipient of the IEEE MTT-S Japan Chapter Young Engineer Award, in 2013.

LEI ZHU (Fellow, IEEE) received the B.Eng. and M.Eng. degrees in radio engineering from the Nanjing Institute of Technology (now Southeast University), Nanjing, China, in 1985 and 1988, respectively, and the Ph.D. degree in electronic engineering from the University of Electro-Communications, Tokyo, Japan, in 1993.

From 1993 to 1996, he was a Research Engineer with Matsushita–Kotobuki Electronics Industries Ltd., Tokyo. From 1996 to 2000, he was a Research Fellow with École Polytechnique de Montreal, Montreal, QC, Canada. From 2000 to 2013, he was an Associate Professor with the School of Electrical and Electronic Engineering, Nanyang Technological University, Singapore. He joined the Faculty of Science and Technology, University of Macau, Macau, China, as a Full Professor, in August 2013, where he has been a Distinguished Professor, since December 2016. From August 2014 to August 2017, he was the Head of the Department of Electrical and Computer Engineering, University of Macau. So far, he has authored or coauthored more than 685 articles in international journals and conference proceedings. His articles have been cited more than 12000 times with the H-index of 55 (source: Scopus). His research interests include microwave circuits, antennas, periodic structures, and computational electromagnetics.

Dr. Zhu served as a member for the IEEE MTT-S Fellow Evaluation Committee, from 2013 to 2015, and IEEE AP-S Fellow Committee, from 2015 to 2017. He was a recipient of the 1993 Achievement Award in Science and Technology (first prize) from the National Education Committee of China, the 1996 Silver Award of Excellent Invention from Matsushita–Kotobuki Electronics Industries Ltd., the 1997 Asia–Pacific Microwave Prize Award, the 2020 FST Research Excellence Award from the University of Macau, and the 2020 Macao Natural Science Award (second prize) from the Science and Technology Development Fund (FDCT), Macau. He served as the General Chair for the 2008 IEEE MTT-S International Microwave Workshop Series on the Art of Miniaturizing RF and Microwave Passive Components, Chengdu, China, and the Technical Program Committee Co-Chair of the 2009 Asia–Pacific Microwave Conference, Singapore. He was an Associate Editor of the IEEE TRANSACTIONS ON MICROWAVE THEORY AND TECHNIQUES, from 2010 to 2013, and IEEE MICROWAVE AND WIRELESS COMPONENTS LETTERS, from 2006 to 2012.

GEYU LU received the B.Sc. degree in electronic sciences and the M.S. degree from Jilin University, Changchun, China, in 1985 and 1988, respectively, and the Dr. (Eng.) degree from Kyushu University, Fukuoka, Japan, in 1998.

He is currently a Professor with Jilin University. His current research interests include the development of chemical sensors and the application of function materials.